Transcriptomic analysis reveals the molecular mechanisms underlying osteoclast differentiation in the estrogen-deficient pullets

Qiaoxian Yue,[*,†,1] Chenxuan Huang,[*,‡,1] Pengyan Song,[*] Siwei Wang,[*,#] Hui Chen,[*] Dehe Wang,[*] Fuwei Li,[‖] and Rongyan Zhou[*,2]

[*]*College of Animal Science and Technology, Hebei Agricultural University, Baoding 071000, China;* [†]*Department of Animal Breeding and Genetics, Swedish University of Agricultural Science, Uppsala 75007, Sweden;* [‡]*Department of Animal Nutrition and Management, Swedish University of Agricultural Science, Uppsala 75007, Sweden;* [#]*Institute of Cereal and Oil Crops, Hebei Academy of Agriculture and Forestry Sciences, Shijiazhuang 050035, China; and* [‖]*Poultry Institute, Shandong Academy of Agricultural Sciences, Jinan 25000, China*

ABSTRACT Several previous reports have suggested that estrogen (**E2**) is a vital signal responsible for the regulation of skeletal homeostasis and bone remodeling in mammals. E2 could efficiently accelerate the growth of medullary bone in pullets during sexual maturity. Furthermore, the low E2 level can strengthen the mechanical bone functions in female hens. However, mechanistic studies to describe the effects of E2 on bone in pullets during the initiation of the puberty period are remaining elusive. Therefore, the aim of this study was to explore the effect of inhibiting E2 biosynthesis on the biomechanical properties and its molecular mechanism during sexual maturity of pullets. In this study, a total of 90 Hy-line Sonia pullets with comparable body weight at 13 wk of age were selected and categorized into 2 separate groups. Daily, 0.5 mg/4 mL of letrozole (**LZ**) was orally administered to the treatment (**TRT**) group and 4 mL of saline to the control (**CON**) group of pullets for 6 wk. Compared with the CON group, a lower plasma E2 level was observed in the TRT group. Furthermore, plasma P, Gla protein (**BGP**), and 1,25-dihydroxy vitamin D3 (**1,25-$(OH)_2D_3$**) levels were markedly suppressed, whereas the plasma alkaline phosphatase (**ALP**) and tartrate-resistant acid phosphatase (**TRAP**) levels were significantly elevated. Moreover, the cortical bone thickness and breaking strength of the tibia and femur, the bone mineral density of the humerus, and the bone mineral content of the humerus as well as the femur were increased significantly. The expression levels of 340 differentially expressed genes (**DEGs**) differed significantly between the CON and TRT group in the tibia at 19 wk of age. Among them, 32 genes were up-regulated, whereas 308 were down-regulated in the TRT group. The variations in candidate genes associated with osteoclast differentiation and cell adhesion may indicate that LZ inhibits E2 biosynthesis, consequently, reduces osteoclast differentiation by suppressing inter-cellular communication and cells attaching to extracellular matrix components. Taken together, the present study demonstrated that inhibiting E2 synthesis during sexual maturity of pullets decreased osteoclast differentiation and considerably enhanced bone quality.

Key words: estrogen, osteoclast, sexual maturity, pullet

2023 Poultry Science 102:102453
https://doi.org/10.1016/j.psj.2022.102453

INTRODUCTION

Bone, as the main structure of animals, plays a pivotal role in the protection, support, movement, and maintains the basis of body shape. Osteoblasts, which are responsible for bone development, and osteoclast, which can mediate the process of bone resorption, must keep in a balanced state for the maintenance of bone health (Sims and Gooi, 2008). It has been well established that the sexual maturation period is a critical time when a rapid increase in bone hyperplasia takes place. For instance, estrogen (**E2**) can regulate longitudinal growth during sexual maturation (Chagin and Sävendahl, 2007). In early puberty, very low levels of E2 promote bone growth, whereas in late puberty, high E2 levels induce growth plate closure, which reduces and halts longitudinal bone growth in rodents and humans (Juul, 2001; Börjesson et al., 2012). The skeleton completely develops during the growing phase in birds, particularly in laying birds, and is based on the longitudinal growth of the long

Received July 28, 2022.
Accepted December 21, 2022.

[1]These authors contributed equally to this work.

[2]Corresponding author: rongyanzhou@126.com

bones of the appendicular skeleton, which is mediated by endochondral ossification (Whitehead, 2004).

Multiple studies have confirmed that E2 exerts an essential effect on the regulation of bone turnover and bone mass in laying hens. There are 3 different types of bones (cortical, trabecular, and medullary bone) in laying birds. The medullary bone is a source of labile calcium for eggshell calcification (Kerschnitzki et al., 2014). As hens approach sexual maturity, the reproductive system becomes functional, and blood E2 concentration gradually increases and remains at a high level during egg production (Whitehead and Fleming, 2000). Osteoclasts, which are necessary for effective mineralized bone resorption, are generated primarily by the fusion of monocyte/macrophage lineage cells (Pereira et al., 2018; McDonald et al., 2021). Classically, osteoclast fusion consists of 4 basic steps: migration, recognition, cell adhesion, and membrane fusion (Søe, 2020). Bone marrow-derived macrophages (**BMMs**), as osteoclast precursors, can regulate RANK (receptor activator of nuclear factor κ B) expression via modulation of the cell adhesion signaling (Mochizuki et al., 2012). According to a reported study on Japanese quails, E2-induced osteoclastogenesis can be regulated in the bone marrow cells via the RANK/RANKL/OPG (RANK/RANK Ligand/Osteoprotegerin) system during medullary bone formation (Hiyama et al., 2019). Moreover, in prepubertal ovariectomy mice, E2 deficiency can promote both maxilla and mandible growth, accompanied by an increase in RANKL/OPG ratio (Omori et al., 2020; Küchler et al., 2021). A low bone turnover in 20-day-old rats treated with E2 for 14 d was due to decreased bone remodeling (Zhang et al., 2012).

The source of the plasma E2 is secreted principally by the ovarian follicles from testosterone via the enzyme, aromatase (Zhao et al., 2016). Letrozole, as an aromatase inhibitor, has been widely used to attenuate E2 synthesis (Bhatnagar, 2007). Orally administered LZ induced low plasma E2 levels in pullets and strengthens bone mechanical functions at both the structural and material levels (Li et al., 2019). LZ can reduce the formation of the medullary bone by inhibiting the synthesis of E2 (Deng et al., 2010). In pre-sexually mature rats treated with LZ, a reduction in bone length and area is observed in males, the opposite effect was observed in females (Pouliot et al., 2013).

The present study aimed to explore the effect of inhibiting E2 biosynthesis on the biomechanical properties and mechanical function of bone during sexual maturity of pullets by detecting plasma hormone and mineral levels. In addition, the potential mechanism by which inhibiting E2 biosynthesis affects osteoclast differentiation and cell adhesion in pullets was also evaluated with the transcriptome analysis of the tibia.

MATERIAL AND METHODS

Animals and Sample Collection

A total of 90 Hy-line Sonia layers were selected at 13 wk old and were housed individually in the conventional cages (400 × 380 × 350 mm) of a 3-tier system in the animal house of Hebei Agricultural University. After a week of pre-feeding, the birds were randomly divided into 2 distinct groups (45 birds per group). Based on the balanced locations, each group consisted of 3 replicates with 15 birds per replication. For 6 consecutive weeks, 4 mL LZ (0.5 mg, S25071, Yuanye Biotechnology Co., Ltd., Shanghai, China) or saline was given as an oral bolus directly into the crop, and serving as the treatment (**TRT**) or control (**CON**) groups, respectively. All birds were raised in the same room. According to the Hy-line Sonia management guide, the temperature was at 20℃ ± 2℃, and the light cycle was 12 h of light and 12 h of dark from 13 to 16 wk, and then increased to 13 h of light at 17 wk, 13.25 h at 18 wk, and 13.5 h at 19 wk. Feed and fresh water were available ad libitum throughout the experiment. The ingredients and chemical composition of the basal diet during the experiment have been shown in Table S1. Body weight of pullets was determined at the beginning and end of the study. Feed intake was recorded weekly throughout the whole experimental period and average daily feed intake and average daily gain were calculated.

Blood samples were collected from eight birds (1 bird was excluded from each group due to underweight) evenly from the 3 replicates per group at week 19. Formerly, the plasma was collected after 3,000 rpm centrifugation for 15 min and stored at −20℃. ELISA kits were used for the measurements of plasma E2, alkaline phosphatase (**ALP**), Gla protein (**BGP**), 1,25-dihydroxy vitamin D3 (**1,25-$(OH)_2D_3$**), and tartrate-resistant acid phosphatase (**TRAP**) level (Shanghai Jianglai Biotechnology Co., Ltd., Shanghai, China). The plasma total calcium (**Ca**) and inorganic phosphorus (**Pi**) level were detected using Ca and P concentration test kits, respectively (C004 and C006, Nanjing Jiancheng Bioengineering Institute, Nanjing, China).

The pullets in the CON group started to produce eggs at 19 wk, whereas the LZ group pullets laid no eggs. At the end of the experiment, the samples of left bones (humerus, femur, and tibia) and the right tibia were collected within 3 h after laying (n = 8), and the muscle and connected tissues were removed. The left bones were used to analyze bone biomechanical properties and mechanical function. The bone weight was measured by an electronic balance (accuracy 0.01 g), and the bone length, bone middle width, and cortical bone thickness were evaluated with a vernier caliper (accuracy 0.1 mm). The cortical thickness was an average of 3 measurements at the breaking location at the mid diaphysis of each bone. To assess the bone breaking strength of the humerus, femur, and tibia, a 3-point bending test was performed by using a Texture Analyzer (TA. XTPlus, Surrey, UK). Each bone was loaded on 2 fulcrum points (4.8 cm apart for the humerus, 6.0 cm apart for the femur, and 6.4 cm apart for the tibia) and a constant force was applied using the Texture Analyzer with a 30 kg load cell until the bone fractured. The breaking strength (g/g) was read as the peak of the curve produced by the connected software, following suitable calibration, and was corrected by the live body weight of

each pullet. The mechanical functions of bone mineral density (**BMD**) and bone mineral content (**BMC**) were analyzed by a small animal dual-energy X-ray bone mineral density and body composition analyzer (iNsight Vet DXA, OsteoSys, Seoul, Korea). The bones were scanned individually, and designated as the interested region containing both cortical and medullary bone, and the measurement took about 25 s. The individual results were analyzed using the Insight software (Version 1.0.6; OsteoSys, Seoul, Korea). The mid-diaphysis of the right tibias with both cortical and medullary bone of each bird was cut into 0.5 cm and immediately snap-frozen in the liquid nitrogen for RNA isolation and next-generation sequencing.

Tissue Preparation and Histology

A 0.5 cm mid-diaphysis of the right tibia of each bird (3 per treatment) was cut and fixed in 10% formalin for 48 h. For further histological analysis, the samples were decalcified in 10% EDTA-2Na (pH = 7.4) for 4 wk. The paraffin sections were then prepared and a 4-μm section of each sample was placed on a glass slide and stained with toluidine blue (**TB**). TB staining was performed to detect proteoglycan changes in the bone matrix deposition. Three sections were examined of each sample, and 3 images were obtained of each section, which were collected by an inverted phase microscope (BDS200-FL, Nikon Corporation, Tokyo, Japan).

RNA Sequencing of Tibia

Three biologically replicate samples of tibias were first ground in liquid nitrogen using a pestle and mortar. The samples came from the CON group (designed as C1, C2, and C3, respectively) with medullary bone formation and the TRT group (designed as LZ1, LZ2, and LZ3, respectively) without medullary bone. Total RNA was then isolated from the tibia tissues using the TRIzol Plus RNA Purification Kit (Invitrogen, Carlsbad, CA, 12183555) following the manufacturer's instructions. Both the concentration and purity of total RNA were estimated using the Qubit RNA Assay Kit (Invitrogen, Q10211) in a Qubit 2.0 Fluorometer (Life Technologies, Carlsbad, CA) and a NanoPhotometer spectrophotometer (IMPLEN, Los Angeles, CA), accordingly. Furthermore, RNA integrity was evaluated via the RNA Nano 6000 Assay Kit (Agilent Technologies, Santa Clara, CA, 5067-1511). The libraries were constructed using the NEBNext Ultra RNA Library Prep Kit for Illumina (NEB, Ipswich, MA, E7530L) following the manufacturer's protocol and were sequenced on an Illumina Hiseq platform and 150-bp paired-end reads were generated.

Analysis of RNA Sequencing Data

For the analysis of RNA sequencing, first, the clean reads were obtained by removing reads containing adapter ploy-N and low-quality reads from the raw data (raw reads). Next, TopHat2 software was used to map reads to the *G. gallus* genome (Gallus_gallus-6a, GCA_000002315.5). Cuffquant and cuffnorm (v2.2.1) were used to estimate the expression levels of all the transcripts and analyze expression levels for mRNAs by calculating FPKM (Trapnell et al., 2012). The resulting *P*-value was adjusted using Benjamini and Hochberg's approach for controlling the false discovery rate. The various differentially expression genes (**DEGs**) were selected between the 2 groups by using the DESeq2 R package when the adjusted *P*-value < 0.01 and the absolute value of the $\log_2$ (fold change) was larger than 1 (Varet et al., 2016). The volcano plot and heatmap of DEGs were clustered using TBtools (version 1.046) (Chen et al., 2020).

Gene Ontology and KEGG Enrichment Analysis

Gene Ontology (**GO**, http://geneontology.org/) enrichment analysis of the DEGs was performed to assess their biological significance using the GOseq R package, and the gene length bias was corrected. Statistically, $P < 0.05$ was considered significant for GO enrichment. KEGG is a database (http://www.genome.jp/kegg/) resource for analyzing the signaling pathway mainly involved in the regulation of DEGs. KOBAS software was used to test the statistical enrichment of DEGs in KEGG pathways (Xie et al., 2011).

Protein−Protein Interaction Network Analysis

A protein−protein interaction network was constructed by using the STRING database (11.5) (https://cn.string-db.org/) with 30-target DEGs. The k-means algorithm clustered the genes into 2 different groups with moderate confidence (cutoff edge = 0.400) in their correlation.

Validation With qRT-PCR

The PrimeScript RT reagent Kit with gDNA Eraser (Takara, Dalian, China) was used for the cDNA synthesis. The information and the amplification efficiency of qRT-PCR primers for Carbonic Anhydrase 2 (***CA2***), Lipase A, Lysosomal Acid Type (***LIPA***), T Cell Immune Regulator 1 (***TCIRG1***), Cathepsin K (***CTSK***), Nuclear Factor of Activated T Cells 1 (***NFATc1***), Zona Pellucida Glycoprotein 1 (***ZP1***), Bone Morphogenetic Protein 7 (***BMP7***), Matrix Extracellular Phosphoglycoprotein (***MEPE***), TIMP Metallopeptidase Inhibitor 4 (***TIMP4***), and Tripartite Motif Containing 25 (***TRIM25***) have been shown in Table S2. The qRT-PCR reaction systems using the EvaGreen qPCR Master Mix (Biotium, Bay Area, CA) and stages using the Q6 Flex Real-Time PCR detection system (Applied Biosystems, Foster City, CA) have been summarized in Tables S3 and S4. The expression

levels of each tested gene were normalized to the expression level of *18S* and calculated by the $2^{-\Delta\Delta Ct}$ method.

Statistical Analysis

The obtained data were statistically analyzed by SPSS version 21.0. The normal distribution and homogeneity of variance were tested. The Student's independent *t* test was employed to reveal the significance between pullets in the CON and TRT groups. *P*-values <0.05 and <0.01 were considered significant differences and extremely significant differences, respectively. The data have been presented as mean ± SD.

RESULTS

Growth Performance

The growth performance of pullets with or without oral administration of LZ has been shown in Table 1. The initial body weight, final body weight, average daily feed intake, and average daily gain exhibited no significant difference between the 2 groups.

Plasma Biochemical Parameters

The descriptive statistics of plasma biochemical parameters with or without oral administration of LZ have been depicted in Table 2. The levels of E2, 1,25 $(OH)_2D_3$, BGP, Pi, and Ca of the TRT pullets were lower than those of CON pullets ($P < 0.01$ and $P < 0.05$). Furthermore, the ALP and TRAP levels in the TRT pullets were significantly elevated ($P < 0.01$).

Bone Biomechanical Properties

The potential effects of oral administration of LZ on bone quality are shown in Table 3. The bone weight, length, and middle width of the tibia, femur, and humerus exhibited no significant difference between the 2 groups. For the tibia, the thickness, breaking strength, BMD and BMC levels were higher in the TRT pullets than the CON pullets ($P < 0.01$). For the femur, different treatments displayed a significant effect on bone thickness, breaking strength and BMC ($P < 0.01$); however, no significant differences were observed on BMD. Compared to the CON pullets, the BMD and BMC of the humerus in the TRT group pullets were considerably greater ($P < 0.05$ and $P < 0.01$), although bone thickness and breaking strength were comparable. Moreover, no medullary bone was observed in the LZ-treated tibias compared to the untreated control (Figure 1).

Table 1. The potential effect of LZ on the growth performance.

Items	CON	TRT
Initial body weight (kg)	1,058.60 ± 65.5	1,067.80 ± 31.0
Final body weight (kg)	1,357.40 ± 75.7	1,366.82 ± 77.5
Average daily feed intake (kg/d)	68.62 ± 2.3	69.95 ± 3.0
Average daily gain (g/d)	7.11 ± 0.4	6.95 ± 0.5

CON, control; LZ, letrozole; TRT, treatment.

Table 2. The effect of LZ on plasma biochemical index.

Items	CON	TRT
E2 (pg/mL)	407.00 ± 31.51^{A}	309.16 ± 55.60^{B}
ALP (ng/mL)	101.28 ± 16.82^{B}	156.42 ± 21.41^{A}
BGP (ng/mL)	9.25 ± 1.07^{a}	8.13 ± 1.20^{b}
1,25-$(OH)_2D_3$ (ng/mL)	28.13 ± 4.14^{A}	20.29 ± 3.15^{B}
TRAP (pg/mL)	439.09 ± 97.06^{B}	538.79 ± 84.57^{A}
Pi (mmol/L)	1.00 ± 0.38^{a}	0.85 ± 0.14^{b}
Ca (mmol/L)	1.58 ± 0.11^{a}	1.46 ± 0.31^{b}

ALP, alkaline phosphatase; BGP, Gla protein; Ca, total calcium; CON, control; E2, estrogen; 1,25-$(OH)_2D_3$, 1,25-dihydroxy vitamin D3; LZ, letrozole; Pi, inorganic phosphorus; TRAP, tartrate-resistant acid phosphatase; TRT, treatment.

The values are represented as mean ± SD (n = 8). Significant differences were analyzed between the CON and TRT groups, *P*-value was considered to be statistically significant with:

$^{a,b}P < 0.05$.

$^{A,B}P < 0.01$.

Quality Control and DEGs Analysis of RNA-Seq Data

Herein, a total of 254 million clean reads and 38.09 G clean bases were obtained with GC content ≥ 50.80%. The average Q30 quality data from the CON and TRT groups were found to be 93.96% and 94.04%, respectively. The average percentage of uniquely mapped reads in each library was 99.81% and 99.82%, respectively (Table S5).

Next, 3 biologically replicate samples of tibias from individuals with higher (CON group) and lower (TRT group) plasma E2 levels were evaluated. To identify the DEGs in the tibia between the 2 groups, we used DESeq2 with FDR < 0.01 and a threshold of |Log2(fold-change)| ≥ 1 for the comparison. In the tibia of the TRT group, a total of 340 DEGs were identified, including 32 up-regulated and 308 down-regulated genes (Figure 2, Table S7).

GO Enrichment Analysis of DEGs

The GO analysis was used to reveal the various biological processes that might be affected by LZ treatment. Of the 340 DEGs, 292 were then divided into 3 major categories: 10 molecular functions (**MFs**), 14 cellular components (**CCs**), and 23 biological processes (**BPs**), as shown in Figure 3 A. The top 19 significant GO function annotation terms (Fisher's exact test, Q-value < 0.05) in the TRT pullets compared to the CON pullets have been shown in Figure 3B. However, in the BP category, metabolic process, cellular process, and developmental process were the key processes found to be involved in response to LZ treatment. The major subcategories were the cholesterol biosynthetic process (GO:0006695), osteoclast differentiation (GO:0030316), bone mineralization (GO:0030282), middle ear morphogenesis (GO:0042474), Leukemia inhibitory factor signaling pathway (GO:0048861), monocyte chemotaxis (GO:0002548), and protein heterotrimerization (GO:0070208). The CC category included enriched

Table 3. The effect of LZ on the bone quality.

Items	Tibia		Femur		Humeral	
	CON	TRT	CON	TRT	CON	TRT
Weight/g	7.51 ± 0.93	8.08 ± 0.63	6.67 ± 0.79	7.25 ± 0.48	2.51 ± 0.57	2.87 ± 0.60
Length/mm	116.64 ± 4.61	117.72 ± 2.98	81.66 ± 3.68	82.91 ± 1.57	76.54 ± 2.12	77.53 ± 1.49
Middle width/mm	7.11 ± 0.47	7.30 ± 0.43	7.86 ± 0.31	8.08 ± 0.39	7.61 ± 0.31	7.82 ± 0.44
Thickness/mm	0.65 ± 0.08^{B}	0.81 ± 0.07^{A}	0.53 ± 0.05^{B}	0.67 ± 0.05^{A}	0.44 ± 0.05	0.53 ± 0.10
Breaking strength/(g/g)	11.83 ± 2.00^{B}	17.73 ± 1.99^{A}	11.21 ± 1.70^{B}	14.74 ± 2.05^{A}	9.43 ± 1.49	11.76 ± 4.30
BMD/(g/cm^2)	0.22 ± 0.02^{B}	0.24 ± 0.02^{A}	0.20 ± 0.03	0.23 ± 0.02	0.13 ± 0.02^{b}	0.15 ± 0.02^{a}
BMC	2.40 ± 0.29^{B}	2.68 ± 0.20^{A}	1.75 ± 0.20^{B}	2.18 ± 0.15^{A}	1.16 ± 0.21^{B}	1.37 ± 0.19^{A}

BMD, bone mineral density; BMC, bone mineral content; CON, control; LZ, letrozole; TRT, treatment.

The values are represented as mean ± SD (n = 8). Significant differences were analyzed between the CON and TRT groups, *P*-value was considered to be statistically significant with:

$^{a,b}P < 0.05$.

$^{A,B}P < 0.01$.

terms such as extracellular space (GO:0005615), extracellular exosome (GO:0070062), extracellular matrix (GO:0031012), interstitial matrix (GO:0005614), and proteinaceous extracellular matrix (GO:0005578), which belong to extracellular region and extracellular region regulated processes. The various genes related to collagen trimer (GO:0005581), endoplasmic reticulum (GO:0005783), and receptor complex (GO:0043235) were mainly involved in the protein-containing complex process. The adherens junction (GO:0005912), fascia adherens (GO:0005916), and focal adhesion (GO:0005925) were found to be significantly enriched in the cell junction category. However, only the carbonate dehydratase activity (GO:0004089) in the MF ontology met the cut-off criteria.

KEGG Pathways Analysis of DEGs

According to the KEGG database, the DEGs were clustered into 5 major biological pathways, which included the cellular processes (52 genes), environmental information processing (146), human diseases (97), metabolism (11), and organismal systems (55) pathways (Figure 4A). Herein, 23 pathway annotations were significantly enriched, and the main identified pathways could regulate steroid biosynthesis (ko00100), sesquiterpenoid as well as triterpenoid biosynthesis (ko00909), nitrogen metabolism (ko00910), synaptic vesicle cycle (ko04721), and osteoclast differentiation (ko04380) (Figure 4B).

Candidate Genes Related to Steroid Biosynthesis

The expression patterns of various genes involved in steroid biosynthesis were analyzed to investigate the potential regulatory mechanisms involved in the oral administration of LZ. A total of 15 DEGs encoding steroid biosynthesis were identified in the tibia (Figure 5). The sesquiterpenoid and triterpenoid biosynthesis pathways can generate cholesterol, which acts as a precursor of the sex hormones, including E2. It has been reported that oral administration of LZ contributes to blocking the biosynthesis of E2 in pullets.

Prediction of the Network

A critical process in osteoclast differentiation, adhesion junction, is the directed migration of the fused precursor cells. The protein−protein interaction network of cell adhesion and osteoclast development markers were predicted to study the possible mechanism by which

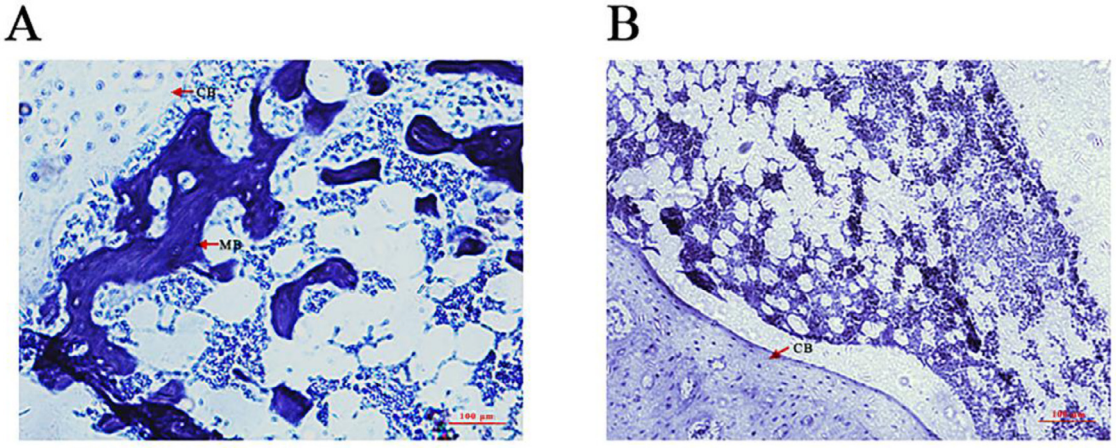

Figure 1. Histological analyses of changes in tibia after LZ treated. Transverse sections of CON (A) and TRT (B) tibia stained with toluidine blue. The scale is 100 μm. Abbreviation: LZ, letrozole; MB, medullary bone; CB, cortical bone.

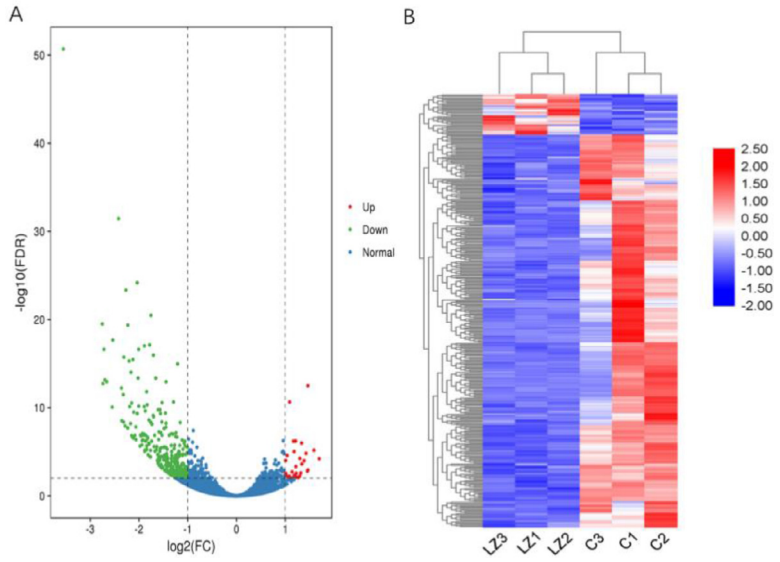

Figure 2. The differential expression of genes extracted from the RNA-Seq data obtained in response to the saline and letrozole treatment. (A) Volcano plot of distribution trends for the various DEGs. A dot represents one DEG, showing the up-regulation highlighted in red, down-regulation in green, and normal-regulation in blue. (B) Heatmap of expression level for all DEGs among the 6 samples. The transition from blue to red strips represents an increase in the gene expression levels. Abbreviation: DEGs, differentially expressed genes.

suppressed E2 can effectively alter bone quality and medullary bone formation (Figure 6). In this study, the majority of the DEGs were found to be down-regulated in the TRT tibia except for the up-regulated *CA2*. The interacting proteins were clustered into 2 distinct groups (regulation of adhesion junction and osteoclast differentiation) with medium confidence. The results indicated several interactions for Syndecan 1 (**SDC1**), Glypican 3 (**GPC3**), Cadherin 2 (**CDH2**), Cadherin 11 (**CDH11**), EPH Receptor A2 (**EPHA2**), Alanyl Aminopeptidase, Membrane (**ANPEP**), Gap Junction Protein Alpha 1 (**GJA1**), Ras Homolog Family Member C (**RHOC**), Fms Related Receptor Tyrosine Kinase 1 (**FLT1**), Msh Homeobox 1 (**MSX1**), Fibroblast Growth Factor 18 (**FGF18**), Fibroblast Growth Factor Receptor 1 and 2 (**FGFR1** and **FGFR2**), and Matrix Metallopeptidase 10 (**MMP10**), which are reported to be involved in the regulation of cell adhesion junction and migration. The various nodes that link osteoclast differentiation to the regulation of the cell adhesion junction were revealed.

Validation by Real-Time PCR

The qRT-PCR analysis was performed to validate the RNA-Seq-identified altered gene expressions. According to the obtained results, the relative expression levels of the 10 genes (ie, *CA2, LIPA, TCIRG1, CTSK, NFATc1, ZP1, MEPE, BMP7, TIMP4*, and *TRIM25*) obtained by qRT-PCR were highly consistent with the RNA-Seq data (Figure 7, Table S6).

DISCUSSION

At the onset of sexual maturity, the elevation in plasma E2 level can effectively stimulate the osteoblasts to produce medullary instead of structural bone, resulting in a significant decline in structural bone development (Whitehead and Fleming, 2000). E2 is a crucial factor involved in the formation of the medullary bone in birds (Hiyama et al., 2012). High estradiol concentrations in late adolescence led to growth plate closure (Börjesson et al., 2012). In prepubertal ovariectomy mice, E2 deficiency can promote both maxilla and mandible growth, accompanied by an increase in RANKL/OPG ratio (Omori et al., 2020; Küchler et al., 2021). The loss of E2 during sexual maturity leads to reduced medullary bone formation (Figure 1). Nonetheless, the TRT pullets with lower plasma E2 levels had greater bone strength than the CON pullets, because of the increased cortical bone thickness, BMC and BMD, which were the results of bone gained on the periosteal surface during puberty. Additionally, compared with untreated capon, bone strength was significantly reduced after exogenous estradiol treatment (Chen et al., 2014). Furthermore, bone quality can be affected by a variety of factors, such as nutrition (Olgun and Aygun, 2016), genetic basis (Raymond et al., 2018), housing systems, and age (Yue et al., 2020). However, the environmental conditions, management, and genetic background used were identical in this study, and there was no significant difference in initial body weight, final body weight, average daily feed intake, or average daily gain between the 2 groups, thus indicating that the change of bone quality was caused by the change of E2.

At day 14 post-E2 treatment, the rats at 20 d of age had lower biomarkers, serum levels of ALP and RatLap (C telopeptide of type 1 collagen), for bone formation and resorption, consequently decreasing bone turnover (Zhang et al., 2012). Consistent with the finding of this study, increasing plasma levels of ALP and TRAP in

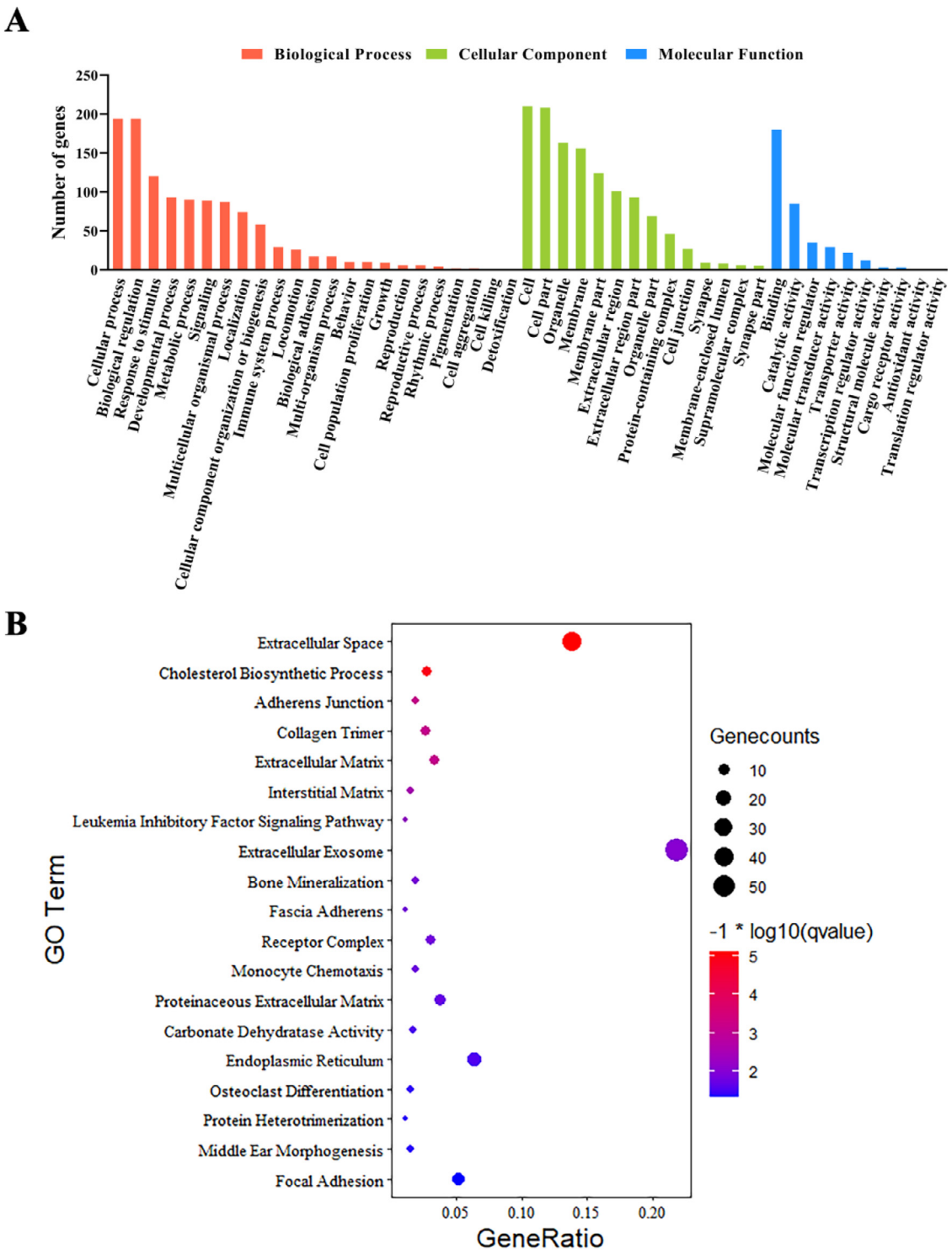

Figure 3. GO annotation and enrichment analysis. (A) GO annotation results for the total number of DEGs (Fisher's exact test, Q-value < 0.05). (B) GO enrichment analysis. The top 19 pathways with minimum Q values (Q-value < 0.05) have been shown. Abbreviations: DEGs, differentially expressed genes; GO, Gene Ontology.

the TRT pullets suggested a significant increase in bone turnover. The CON pullets started to produce eggs at 19 wk, which leads to more calcium being absorbed from the intestines and bones to form eggshells, thereby the plasma calcium concentration was higher than that of non-laying TRT pullets. The pullets treated with LZ significantly decreased the concentration of BGP, as well as plasma E2 level. BGP can participate in regulating normal bone and matrix mineralization (Brennan-Speranza and Conigrave, 2015; Fusaro et al., 2018). As an active form of vitamin D, $1,25(OH)_2D_3$ can exhibit a critical effect on osteogenic differentiation and mineralization of chicken mesenchymal stem cells depending on the cell stage and maturity (Chen et al., 2021).

The current study provides a transcriptome analysis of the various genes and pathway involved in bone development in response to suppressed E2 levels in pubescent hens. The DEGs involved in the steroid biosynthesis,

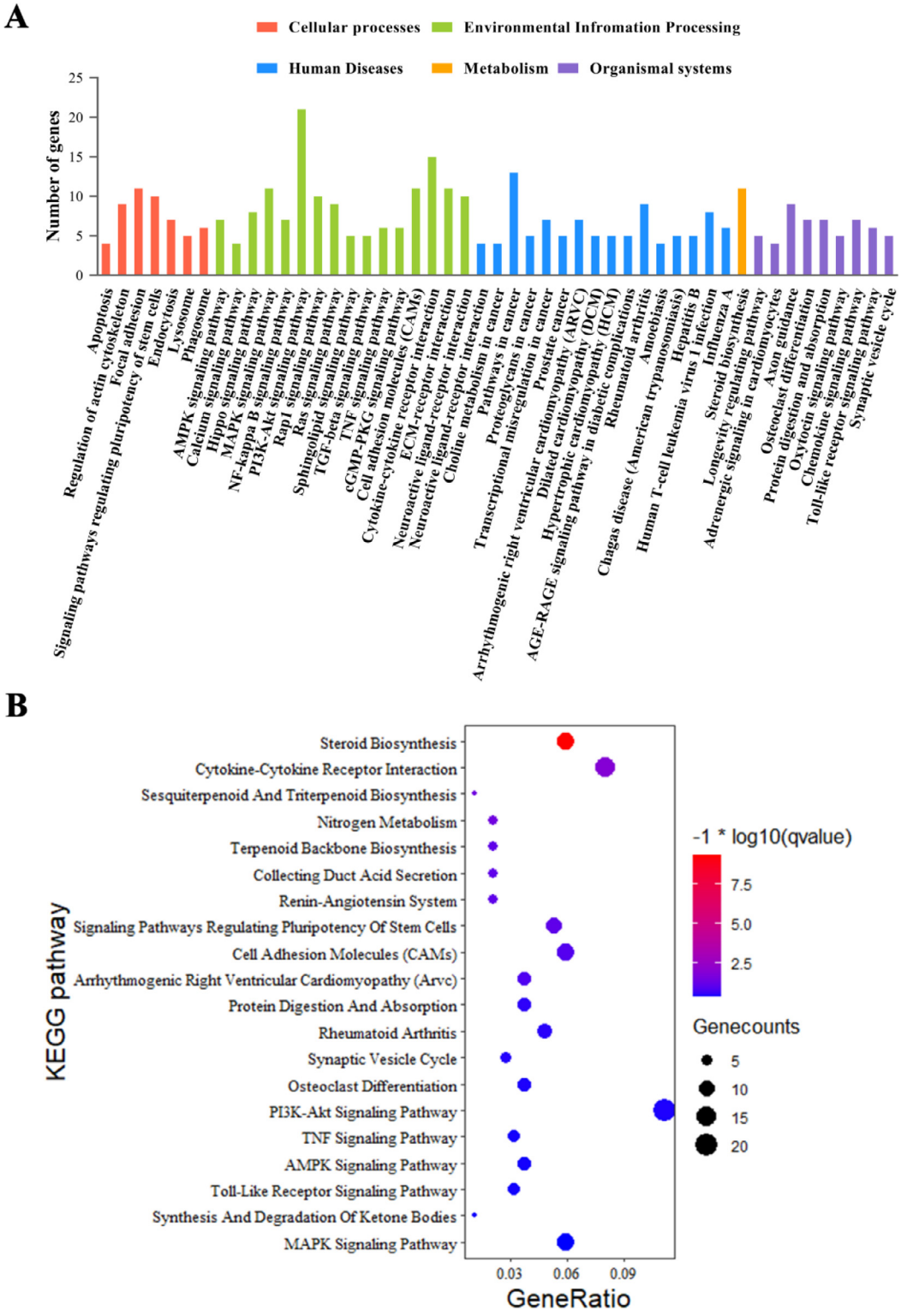

Figure 4. KEGG annotation and enrichment analysis. (A) KEGG pathway annotation for the total number of DEGs ($Q < 0.05$). (B) KEGG enrichment analysis. The top 15 pathways with minimum Q value (Q value < 0.4) have been depicted.

sesquiterpenoid and triterpenoid biosynthesis, and terpenoid backbone biosynthesis were found to be substantially down-regulated in the TRT group, which suggested that oral administration of LZ could successfully inhibit E2 synthesis. Farnesyl-PP can also synthesize cholesterol by using desmosome sterols or 7-dehydrocholesterol (Shahoei and Nelson, 2019), whereas cholesterol functions as a precursor molecule in the synthesis of different sex hormones, including testosterone, E2s, and progesterone (Lee et al., 2019).

Osteoblasts and osteoclasts, respectively, regulate the processes of osteogenesis and resorption which are primarily responsible for maintaining bone homeostasis. The results of this study showed that for hens in the

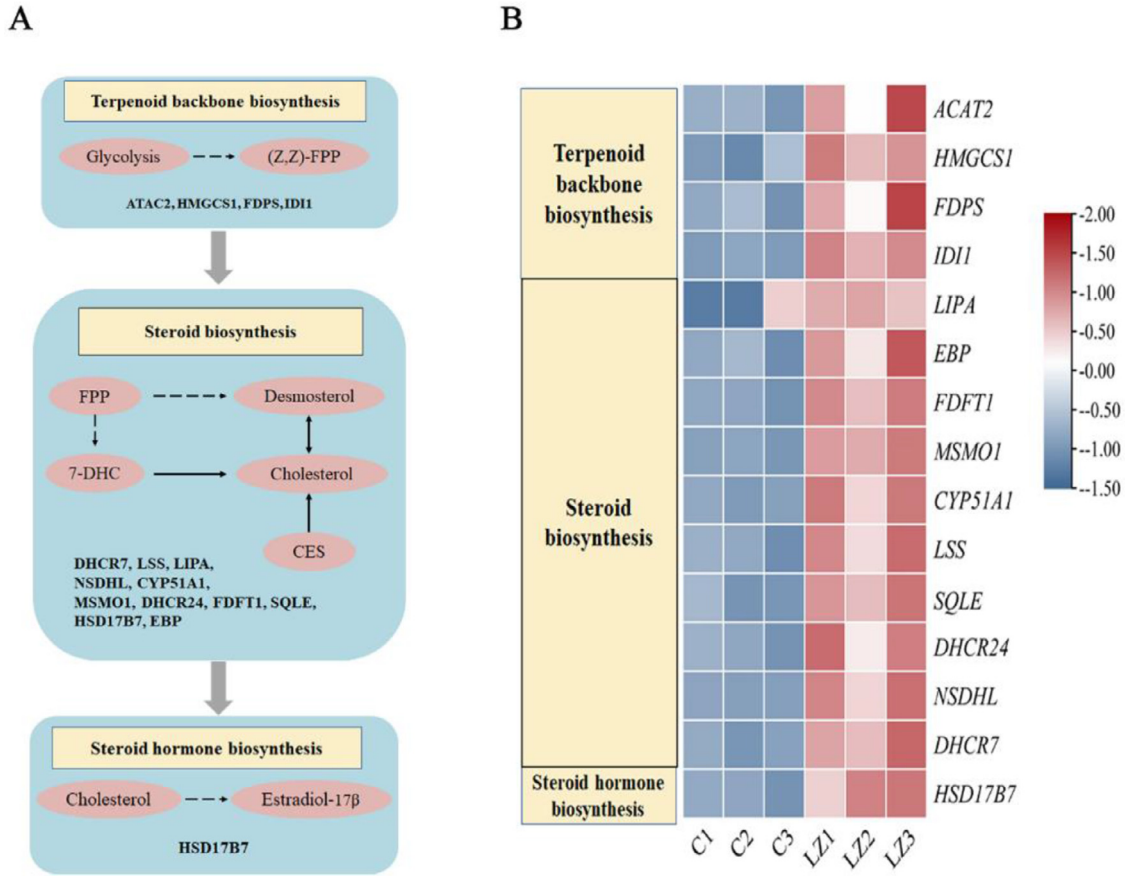

Figure 5. The main pathway and heatmap of DEGs related to steroid biosynthesis in tibia. (A) Terpenoid backbone biosynthesis, steroid biosynthesis, and steroid hormone biosynthesis pathways. (B) Heatmap of the various DEGs involved in terpenoid backbone biosynthesis, steroid biosynthesis and steroid hormone biosynthesis. The scale bar has been shown as the -$\log_2$(FPKM+1) value. Abbreviation: DEGs, differentially expressed genes.

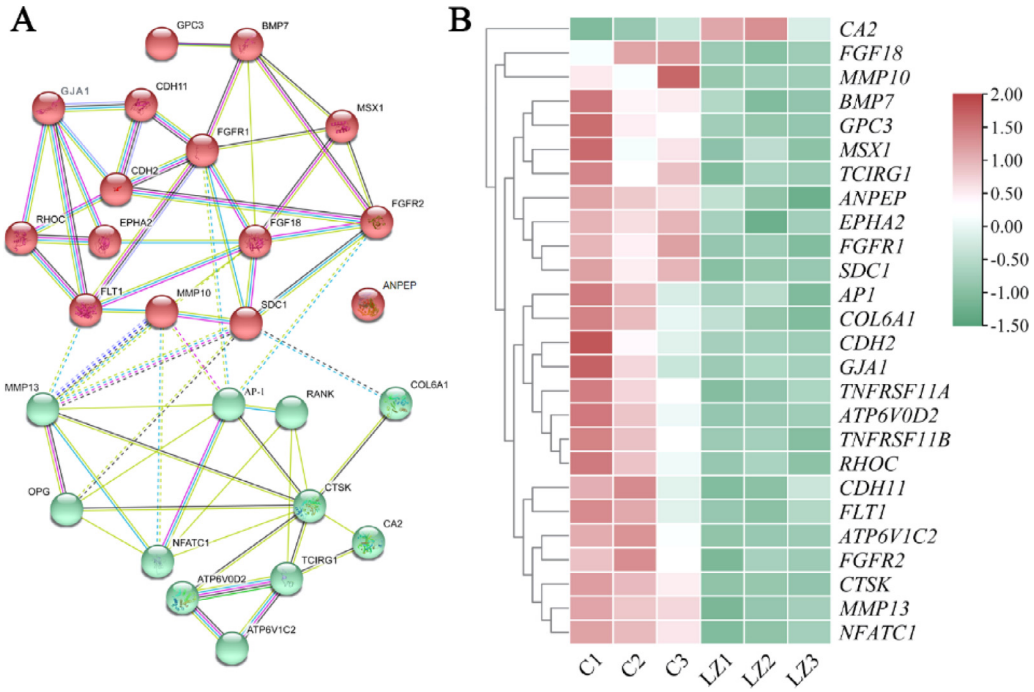

Figure 6. The DEGs involved in the regulation of cell adhesion and osteoclast differentiation. (A) Predicted protein−protein interaction network involved in the regulation of cell adhesion (red balls) and osteoclast differentiation markers (green balls). The network of interaction proteins was clustered into 2 distinct parts using the k-means method. (B) Heatmap of DEGs involved in cell adhesion and osteoclast differentiation. Abbreviation: DEGs, differentially expressed genes.

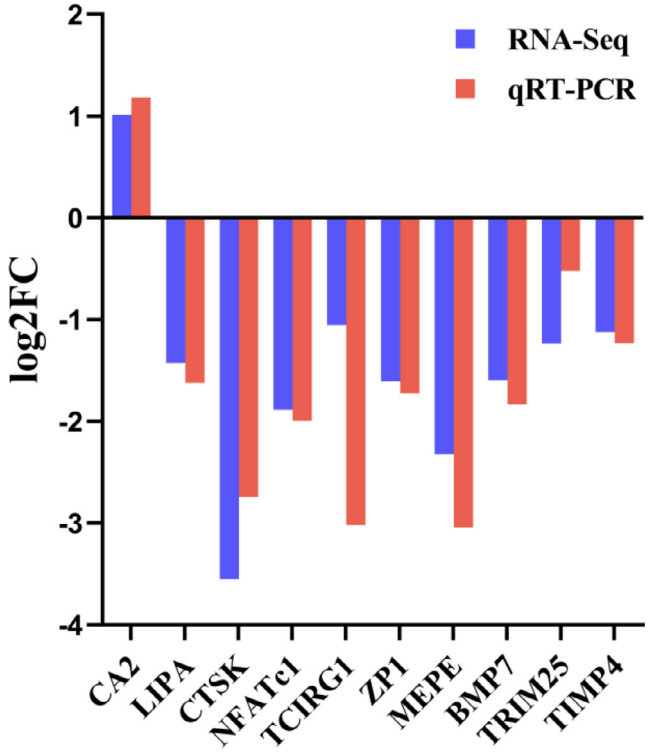

Figure 7. Illustration of qRT-PCR and RNA-Seq for the selected differentially expressed genes. Abbreviations: *BMP7*, Bone Morphogenetic Protein 7; *CA2*, Carbonic Anhydrase 2; *CTSK*, Cathepsin K; *LIPA*, Lipase A, Lysosomal Acid Type; *MEPE*, Matrix Extracellular Phosphoglycoprotein; *NFATc1*, Nuclear Factor of Activated T Cells 1; *TCIRG1*, T Cell Immune Regulator 1; *TIMP4*, TIMP Metallopeptidase Inhibitor 4; *TRIM25*, Tripartite Motif Containing 25; *ZP1*, Zona Pellucida Glycoprotein 1.

TRT group, both osteoclast differentiation and maturation were suppressed by reducing gene expression of cell adhesion contributing to intercellular junction formation. As a kind of proteoglycan, heparan sulfate proteoglycans can actively participate in the formation of bone matrix and maintain the stability of the internal structure and function of the bone tissue. The 2 primary heparan sulfate proteoglycans families are GPCs and SDCs. SDC1 is crucial cell surface adhesion molecule that contributes to the maintenance cell morphology. Furthermore, SDC1 has been reported as a unique regulator of bone-cell communication, as osteoclasts lacking SDC1 have diminished differentiation and bone resorption potential (Kim et al., 2018; Timmen et al., 2020). GPC3 is an important bone co-regulator, and GPC3-deficient mice resulted in reduced mandibular growth and decreased osteoclast differentiation (Viviano et al., 2005; Mian et al., 2017). Cadherins are cell adhesion molecules, which are homologous to calcium-dependent glycoproteins. Up-regulated expression of CDH11 can mediate the adhesion between osteoclast precursors and up-regulated specific collagen production (Qian et al., 2021). CDH2 can also regulate the number and differentiation of osteoprogenitors in ovariectomized mice, possibly by stabilizing cell-cell adhesion and /or signaling (Lai et al., 2006). Similar to other tissues, gap junction intercellular communication is a key component of bone intercellular communication. The role and mechanism of GJA1 in bone have been described in detail in a previous study. In brief, GJA1 can function as a key regulator of bone growth and homeostasis (Stains and Civitelli, 2016). CDH2 also contributes to GJA1-mediated gap junction in BMSCs (Sinha et al., 2021). ANPEP is a specific glycosylated type Ⅱ membrane protein highly expressed in the monocytes, macrophages, and dendritic cells. ANPEP can aid in the regulation of cell adhesion, migration, and other functions, which can control cell-cell fusion by modulating the fusion-regulatory protein in osteoclastogenesis (Licona-Limón et al., 2015; Ghosh et al., 2021). Lower expression levels of these genes in the TRT group indicated decreased osteoclast migration and adhesion.

Rho GTPase can impact actin and myosin activity and cell adhesion to regulate cell migration (Zhao et al., 2019). RhoC is a vital member of the Rho GTPase family and is responsible for cytoskeletal reorganization and cell motility (Guan et al., 2018; Thomas et al., 2019). The intracellular domain fragment of EPHA3 can bind to non-muscle myosin ⅡA (**NM**Ⅱ**A**) and phosphorylated NMⅡA, thereby promoting NMⅡA filament disassembly and cytoskeletal rearrangement (Javier-Torrent et al., 2019). Interestingly, mutations within the EPHA2 tyrosine kinase domain can lead to the expression disorders of several cytoskeleton-associated proteins (Zhou et al., 2021). As key members of the MMP family, MMP10 and MMP13 are the main proteases involved in ECM protein degradation and MMP13 mainly cleaves type Ⅰ, Ⅱ, and Ⅲ collagens. TGFB3 was reported to affect MMP13 in a mice liver fibrosis model (Guo et al., 2021). Moreover, initial cells can modulate *Msx1* and *Msx2* genes to regulate calmodulin-mediated adhesion (Lincecum et al., 1998). Furthermore, Msx1 could directly bind to and up-regulate the expression of FGF18, thus activating MAPK signaling pathway (Yang et al., 2020). Also, FGF18 enhanced chondrocyte and breast cancer cell migration (Song et al., 2018; Yao et al., 2019). Therefore, inhibition of E2 biosynthesis during puberty was predicted to be closely related to the regulation of cell adhesion, migration, and osteoclastogenesis markers, as their expression levels changed under different E2 conditions.

CONCLUSIONS

Taken together, LZ effectively suppresses the E2 biosynthesis during puberty in pullets. Consequently, E2 biosynthesis inhibition enhances bone quality, including cortical bone thickness, bone mineral content, and bone mineral density. The suppression of E2 in pubertal pullets significantly suppressed osteoclast differentiation by reducing gene expression of cell adhesion junctions.

ACKNOWLEDGMENTS

We thank the members of our group for their help during the sample collection.

This research was supported by National Natural Science Foundation of China (32272922), the Hebei Province Graduate Innovation Funding Project (grant number CXZZBS2022051, 2022-2023), the China Agriculture Research System of MOF and MARA (grant number CARS-40), the Major Scientific and Technological Innovation Project (MSTIP): The Research and Demonstration on Key Technologies of Precision Breeding and Management of Laying Hens (grant number 2019JZZY020611), and the State Scholarship Fund of the China Scholarship Council (grant number 202010230008).

Ethical Approval: The practices adopted for the care and use of animals for this study complied with the institutional and national criteria were authorized by the Animal Use and Ethical Committee of Hebei Agricultural University (HB/2019/03). Several steps were taken to minimize animal pain, suffering, and distress.

DISCLOSURES

The authors declare no conflict of interest.

SUPPLEMENTARY MATERIALS

Supplementary material associated with this article can be found in the online version at doi:10.1016/j.psj.2022.102453.

REFERENCES

Bhatnagar, A. S. 2007. The discovery and mechanism of action of letrozole. Breast Cancer Res. Treat. 105(Suppl 1):7–17.

Börjesson, A. E., S. H. Windahl, E. Karimian, E. E. Eriksson, M. K. Lagerquist, C. Engdahl, M. C. Antal, A. Krust, P. Chambon, L. Sävendahl, and C. Ohlsson. 2012. The role of estrogen receptor-α and its activation function-1 for growth plate closure in female mice. Am. J. Physiol. Endocrinol. Metab. 302: E1381–E1389.

Brennan-Speranza, T. C., and A. D. Conigrave. 2015. Osteocalcin: an osteoblast-derived polypeptide hormone that modulates whole body energy metabolism. Calcif. Tissue Int. 96:1–10.

Chagin, A. S., and L. Sävendahl. 2007. Estrogens and growth: review. Pediatr. Endocrinol. Rev. 4:329–334.

Chen, C., R. Adhikari, D. L. White, and W. K. Kim. 2021. Role of 1,25-dihydroxyvitamin D3 on osteogenic differentiation and mineralization of chicken mesenchymal stem cells. Front. Physiol. 12:479596.

Chen, C., H. Chen, Y. Zhang, H. R. Thomas, M. H. Frank, Y. He, and R. Xia. 2020. TBtools: an integrative toolkit developed for interactive analyses of big biological data. Mol. Plant. 13:1194–1202.

Chen, S. Y., T. Y. Li, C. H. Tsai, D. Y. Lo, and K. L. Chen. 2014. Gender, caponization and exogenous estrogen effects on lipids, bone and blood characteristics in Taiwan country chickens. Anim. Sci. J. 85:305–312.

Deng, Y. F., X. X. Chen, Z. L. Zhou, and J. F. Hou. 2010. Letrozole inhibits the osteogenesis of medullary bone in prelay pullets. Poult. Sci. 89:917–923.

Fusaro, M., M. Gallieni, A. Aghi, G. Iervasi, M. Rizzo, A. Stucchi, M. Noale, G. Tripepi, T. Nickolas, N. Veronese, F. Fabris, S. Giannini, L. Calo, A. Piccoli, M. Mereu, L. Cosmai, A. Ferraro, F. Magonara, M. Spinello, S. Sella, and M. Plebani. 2018. Cigarette smoking is associated with decreased bone Gla-protein (BGP) levels in hemodialysis patients. Curr. Vasc. Pharmacol. 16:603–609.

Ghosh, M., T. Kelava, I. V. Madunic, I. Kalajzic, and L. H. Shapiro. 2021. CD13 is a critical regulator of cell-cell fusion in osteoclastogenesis. Sci. Rep. 11:10736.

Guan, X., S. Chen, and Y. Zhao. 2018. The role of RhoC in malignant tumor invasion, metastasis and targeted therapy. Histol. Histopathol. 33:255–260.

Guo, J., W. Liu, Z. Zeng, J. Lin, X. Zhang, and L. Chen. 2021. Tgfb3 and Mmp13 regulated the initiation of liver fibrosis progression as dynamic network biomarkers. J. Cell. Mol. Med. 25:867–879.

Hiyama, S., T. Sugiyama, S. Kusuhara, and T. Uchida. 2012. Evidence for estrogen receptor expression during medullary bone formation and resorption in estrogen-treated male Japanese quails (Coturnix coturnix japonica). J. Vet. Sci. 13:223–227.

Hiyama, S., M. Yokoi, Y. Akagi, Y. Kadoyama, K. Nakamori, K. Tsuga, T. Uchida, and R. Terayama. 2019. Osteoclastogenesis from bone marrow cells during estrogen-induced medullary bone formation in Japanese quails. J. Mol. Histol. 50:389–404.

Javier-Torrent, M., S. Marco, D. Rocandio, M. Pons-Vizcarra, P. W. Janes, M. Lackmann, J. Egea, and C. A. Saura. 2019. Presenilin/γ-secretase-dependent EphA3 processing mediates axon elongation through non-muscle myosin IIA. eLife 8:e43646.

Juul, A. 2001. The effects of oestrogens on linear bone growth. Hum. Reprod. Update. 7:303–313.

Kerschnitzki, M., T. Zander, P. Zaslansky, P. Fratzl, R. Shahar, and W. Wagermaier. 2014. Rapid alterations of avian medullary bone material during the daily egg-laying cycle. Bone 69:109–117.

Kim, J.-M., K. Lee, M. Y. Kim, H.-I. Shin, and D. Jeong. 2018. Suppressive effect of Syndecan ectodomains and N-desulfated heparins on osteoclastogenesis via direct binding to macrophage-colony stimulating factor. Cell Death Dis. 9:1119.

Küchler, E. C., R. M. de Lara, M. A. Omori, G. Marañón-Vásquez, F. Baratto-Filho, P. Nelson-Filho, M. B. S. Stuani, M. Blanck-Lubarsch, A. Schroeder, P. Proff, and C. Kirschneck. 2021. Effects of estrogen deficiency during puberty on maxillary and mandibular growth and associated gene expression—an μCT study on rats. Head Face Med. 17:14.

Lai, C. F., S. L. Cheng, G. Mbalaviele, C. Donsante, M. Watkins, G. L. Radice, and R. Civitelli. 2006. Accentuated ovariectomy-induced bone loss and altered osteogenesis in heterozygous N-cadherin null mice. J. Bone Miner. Res. 21:1897–1906.

Lee, G., S. Lee, N. Ha, Y. Kho, K. Park, P. Kim, B. Ahn, S. Kim, and K. Choi. 2019. Effects of gemfibrozil on sex hormones and reproduction related performances of Oryzias latipes following long-term (155 d) and short-term (21 d) exposure. Ecotoxicol. Environ. Saf. 173:174–181.

Li, Q., J. Xia, S. Wang, Z. Zhou, and Z. Li. 2019. Letrozole induced changes in bone mineral properties and mechanical functions of laying hens. Poult. Sci. 98:2562–2569.

Licona-Limón, I., C. A. Garay-Canales, O. Muñoz-Paleta, and E. Ortega. 2015. CD13 mediates phagocytosis in human monocytic cells. J. Leukoc. Biol. 98:85–98.

Lincecum, J. M., A. Fannon, K. Song, Y. Wang, and D. A. Sassoon. 1998. Msh homeobox genes regulate cadherin-mediated cell adhesion and cell-cell sorting. J. Cell. Biochem. 70:22–28.

McDonald, M. M., W. H. Khoo, P. Y. Ng, Y. Xiao, J. Zamerli, P. Thatcher, W. Kyaw, K. Pathmanandavel, A. K. Grootveld, I. Moran, D. Butt, A. Nguyen, A. Corr, S. Warren, M. Biro, N. C. Butterfield, S. E. Guilfoyle, D. Komla-Ebri, M. R. G. Dack, H. F. Dewhurst, J. G. Logan, Y. Li, S. T. Mohanty, N. Byrne, R. L. Terry, M. K. Simic, R. Chai, J. M. W. Quinn, S. E. Youlten, J. A. Pettitt, D. Abi-Hanna, R. Jain, W. Weninger, M. Lundberg, S. Sun, F. H. Ebetino, P. Timpson, W. M. Lee, P. A. Baldock, M. J. Rogers, R. Brink, G. R. Williams, J. H. D. Bassett, J. P. Kemp, N. J. Pavlos, P. I. Croucher, and T. G. Phan. 2021. Osteoclasts recycle via osteomorphs during RANKL-stimulated bone resorption. Cell. 184:1330–1347.e1313.

Mian, M., S. Ranjitkar, G. C. Townsend, and P. J. Anderson. 2017. Alterations in mandibular morphology associated with glypican 1 and glypican 3 gene mutations. Orthod. Craniofac. Res. 20:183–187.

Mochizuki, A., M. Takami, Y. Miyamoto, T. Nakamaki, S. Tomoyasu, Y. Kadono, S. Tanaka, T. Inoue, and R. Kamijo. 2012. Cell adhesion signaling regulates RANK expression in osteoclast precursors. PLoS One. 7:e48795.

Olgun, O., and A. Aygun. 2016. Nutritional factors affecting the breaking strength of bone in laying hens. World Poult. Sci. J. 72:821–832.
Omori, M. A., G. A. Marañón-Vásquez, P. C. Romualdo, E. C. Martins Neto, M. B. S. Stuani, M. A. N. Matsumoto, P. Nelson-Filho, P. Proff, J. E. León, C. Kirschneck, and E. C. Küchler. 2020. Effect of ovariectomy on maxilla and mandible dimensions of female rats. Orthod. Craniofac. Res. 23:342–350.
Pereira, M., E. Petretto, S. Gordon, J. H. D. Bassett, G. R. Williams, and J. Behmoaras. 2018. Common signalling pathways in macrophage and osteoclast multinucleation. J. Cell Sci. 131:jcs216267.
Pouliot, L., M. Schneider, M. DeCristofaro, R. Samadfam, S. Y. Smith, and D. A. Beckman. 2013. Assessment of a nonsteroidal aromatase inhibitor, letrozole, in juvenile rats. Birth Defects Res. B Dev. Reprod. Toxicol. 98:374–390.
Qian, J., Z.-C. Gong, Y.-N. Zhang, H.-H. Wu, J. Zhao, L.-T. Wang, L.-J. Ye, D. Liu, W. Wang, X. Kang, J. Sheng, W. Xu, X.-L. Liu, J. Wu, and W. Zheng. 2021. Lactic acid promotes metastatic niche formation in bone metastasis of colorectal cancer. Cell Commun. Signal. 19:9.
Raymond, B., A. M. Johansson, H. A. McCormack, R. H. Fleming, M. Schmutz, I. C. Dunn, and D. J. De Koning. 2018. Genome-wide association study for bone strength in laying hens. J. Anim. Sci. 96:2525–2535.
Shahoei, S. H., and E. R. Nelson. 2019. Nuclear receptors, cholesterol homeostasis and the immune system. J. Steroid Biochem. Mol. Biol. 191:105364.
Sims, N. A., and J. H. Gooi. 2008. Bone remodeling: Multiple cellular interactions required for coupling of bone formation and resorption. Semin. Cell Dev. Biol. 19:444–451.
Sinha, G., A. I. Ferrer, S. Ayer, M. H. El-Far, S. H. Pamarthi, Y. Naaldijk, P. Barak, O. A. Sandiford, B. M. Bibber, G. Yehia, S. J. Greco, J.-G. Jiang, M. Bryan, R. Kumar, N. M. Ponzio, J.-P. Etchegaray, and P. Rameshwar. 2021. Specific N-cadherin-dependent pathways drive human breast cancer dormancy in bone marrow. Life Sci. Alliance 4:e202000969.
Søe, K. 2020. Osteoclast fusion: physiological regulation of multinucleation through heterogeneity-potential implications for drug sensitivity. Int. J. Mol. Sci. 21:7717.
Song, N., J. Zhong, Q. Hu, T. Gu, B. Yang, J. Zhang, J. Yu, X. Ma, Q. Chen, J. Qi, Y. Liu, W. Su, Z. Feng, X. Wang, and H. Wang. 2018. FGF18 enhances migration and the epithelial-mesenchymal transition in breast cancer by regulating Akt/GSK3β/B-catenin signaling. Cell. Physiol. Biochem. 49:1019–1032.
Stains, J. P., and R. Civitelli. 2016. Connexins in the skeleton. Semin. Cell Dev. Biol. 50:31–39.
Thomas, P., A. Pranatharthi, C. Ross, and S. Srivastava. 2019. RhoC: a fascinating journey from a cytoskeletal organizer to a Cancer stem cell therapeutic target. J. Exp. Clin. Cancer Res. 38:328.
Timmen, M., H. Hidding, M. Götte, T. E. Khassawna, D. Kronenberg, and R. Stange. 2020. The heparan sulfate proteoglycan Syndecan-1 influences local bone cell communication via the RANKL/OPG axis. Sci. Rep. 10:20510.
Trapnell, C., A. Roberts, L. Goff, G. Pertea, D. Kim, D. R. Kelley, H. Pimentel, S. L. Salzberg, J. L. Rinn, and L. Pachter. 2012. Differential gene and transcript expression analysis of RNA-seq experiments with TopHat and Cufflinks. Nat. Protoc. 7:562–578.
Varet, H., L. Brillet-Gueguen, J. Y. Coppee, and M. A. Dillies. 2016. SARTools: a DESeq2-and EdgeR-based R pipeline for comprehensive differential analysis of RNA-Seq Data. PLoS One 11: e0157022.
Viviano, B. L., L. Silverstein, C. Pflederer, S. Paine-Saunders, K. Mills, and S. Saunders. 2005. Altered hematopoiesis in glypican-3-deficient mice results in decreased osteoclast differentiation and a delay in endochondral ossification. Dev. Biol. 282:152–162.
Whitehead, C. C. 2004. Overview of bone biology in the egg-laying hen. Poult. Sci. 83:193–199.
Whitehead, C. C., and R. H. Fleming. 2000. Osteoporosis in cage layers. Poult. Sci. 79:1033–1041.
Xie, C., X. Z. Mao, J. J. Huang, Y. Ding, J. M. Wu, S. Dong, L. Kong, G. Gao, C. Y. Li, and L. P. Wei. 2011. KOBAS 2.0: a web server for annotation and identification of enriched pathways and diseases. Nucleic Acids Res. 39:W316–W322.
Yang, Y., X. Zhu, X. Jia, W. Hou, G. Zhou, Z. Ma, B. Yu, Y. Pi, X. Zhang, J. Wang, and G. Wang. 2020. Phosphorylation of Msx1 promotes cell proliferation through the Fgf9/18-MAPK signaling pathway during embryonic limb development. Nucleic Acids Res. 48:11452–11467.
Yao, X., J. zhang, X. Jing, Y. Ye, J. Guo, K. Sun, and F. Guo. 2019. Fibroblast growth factor 18 exerts anti-osteoarthritic effects through PI3K-AKT signaling and mitochondrial fusion and fission. Pharmacol. Res. 139:314–324.
Yue, Q. X., H. Chen, Y. J. Xu, C. X. Huang, J. Z. Xi, R. Y. Zhou, L. J. Xu, H. Wang, and Y. Chen. 2020. Effect of housing system and age on products and bone properties of Taihang chickens. Poult. Sci. 99:1341–1348.
Zhang, J., O. P. Lazarenko, X. Wu, Y. Tong, M. L. Blackburn, H. Gomez-Acevedo, K. Shankar, T. M. Badger, M. J. Ronis, and J. R. Chen. 2012. Differential effects of short term feeding of a soy protein isolate diet and estrogen treatment on bone in the prepubertal rat. PLoS One. 7:e35736.
Zhao, H., L. Zhou, A. J. Shangguan, and S. E. Bulun. 2016. Aromatase expression and regulation in breast and endometrial cancer. J. Mol. Endocrinol. 57:R19–R33.
Zhao, Z., K. Liu, X. Tian, M. Sun, N. Wei, X. Zhu, H. Yang, T. Wang, G. Jiang, and K. Chen. 2019. Effects of RhoC downregulation on the angiogenesis characteristics of myeloma vascular endothelial cells. Cancer Med. 8:3502–3510.
Zhou, Y., T. M. Bennett, P. A. Ruzycki, and A. Shiels. 2021. Mutation of the EPHA2 tyrosine-kinase domain dysregulates cell pattern formation and cytoskeletal gene expression in the lens. Cells. 10:2606.